

Measurement of the Decay $B_s^0 \rightarrow D_s^- \pi^+$ and Evidence for $B_s^0 \rightarrow D_s^\mp K^\pm$ in e^+e^- Annihilation at $\sqrt{s} \sim 10.87$ GeV

R. Louvot,¹⁸ J. Wicht,⁹ O. Schneider,¹⁸ I. Adachi,⁹ H. Aihara,⁴² K. Arinstein,¹ V. Aulchenko,¹ T. Aushev,^{18,13} A. M. Bakich,³⁸ V. Balagura,¹³ A. Bay,¹⁸ V. Bhardwaj,³³ U. Bitenc,¹⁴ A. Bondar,¹ A. Bozek,²⁷ M. Bračko,^{20,14} T. E. Browder,⁸ A. Chen,²⁴ B. G. Cheon,⁷ R. Chistov,¹³ I.-S. Cho,⁴⁷ Y. Choi,³⁷ J. Dalseno,⁹ M. Danilov,¹³ M. Dash,⁴⁶ A. Drutskoy,³ W. Dungel,¹¹ S. Eidelman,¹ N. Gabyshev,¹ P. Goldenzweig,³ B. Golob,^{19,14} H. Ha,¹⁶ J. Haba,⁹ K. Hayasaka,²² H. Hayashii,²³ M. Hazumi,⁹ Y. Hoshi,⁴¹ W.-S. Hou,²⁶ H. J. Hyun,¹⁷ T. Iijima,²² K. Inami,²² A. Ishikawa,³⁴ H. Ishino,^{43,*} R. Itoh,⁹ M. Iwasaki,⁴² N. J. Joshi,³⁹ D. H. Kah,¹⁷ J. H. Kang,⁴⁷ N. Katayama,⁹ H. Kawai,² T. Kawasaki,²⁹ H. Kichimi,⁹ S. K. Kim,³⁶ Y. I. Kim,¹⁷ Y. J. Kim,⁶ K. Kinoshita,³ S. Korpar,^{20,14} P. Krizán,^{19,14} P. Krokovny,⁹ R. Kumar,³³ A. Kuzmin,¹ Y.-J. Kwon,⁴⁷ S.-H. Kyeong,⁴⁷ J. S. Lange,⁵ J. S. Lee,³⁷ M. J. Lee,³⁶ S. E. Lee,³⁶ T. Lesiak,^{27,4} J. Li,⁸ A. Limosani,²¹ S.-W. Lin,²⁶ D. Liventsev,¹³ F. Mandl,¹¹ A. Matyja,²⁷ S. McOnie,³⁸ T. Medvedeva,¹³ K. Miyabayashi,²³ H. Miyake,³² H. Miyata,²⁹ Y. Miyazaki,²² R. Mizuk,¹³ T. Mori,²² E. Nakano,³¹ M. Nakao,⁹ S. Nishida,⁹ O. Nitoh,⁴⁵ S. Ogawa,⁴⁰ T. Ohshima,²² S. Okuno,¹⁵ H. Ozaki,⁹ G. Pakhlova,¹³ C. W. Park,³⁷ H. K. Park,¹⁷ R. Pestotnik,¹⁴ L. E. Piilonen,⁴⁶ H. Sahoo,⁸ Y. Sakai,⁹ J. Schümann,⁹ A. J. Schwartz,³ A. Sekiya,²³ K. Senyo,²² M. E. Sevier,²¹ M. Shapkin,¹² J.-G. Shiu,²⁶ J. B. Singh,³³ A. Somov,³ S. Stanič,³⁰ M. Starič,¹⁴ K. Sumisawa,⁹ T. Sumiyoshi,⁴⁴ M. Tanaka,⁹ G. N. Taylor,²¹ Y. Teramoto,³¹ I. Tikhomirov,¹³ K. Trabelsi,⁹ S. Uehara,⁹ T. Uglov,¹³ Y. Unno,⁷ S. Uno,⁹ Y. Usov,¹ G. Varner,⁸ K. Vervink,¹⁸ C. C. Wang,²⁶ C. H. Wang,²⁵ P. Wang,¹⁰ X. L. Wang,¹⁰ Y. Watanabe,¹⁵ R. Wedd,²¹ E. Won,¹⁶ B. D. Yabsley,³⁸ Y. Yamashita,²⁸ M. Yamauchi,⁹ Z. P. Zhang,³⁵ V. Zhilich,¹ V. Zhulanov,¹ T. Zivko,¹⁴ A. Zupanc,¹⁴ N. Zwahlen,¹⁸ and O. Zyukova¹

(The Belle Collaboration)

¹*Budker Institute of Nuclear Physics, Novosibirsk*

²*Chiba University, Chiba*

³*University of Cincinnati, Cincinnati, Ohio 45221*

⁴*T. Kościuszko Cracow University of Technology, Krakow*

⁵*Justus-Liebig-Universität Gießen, Gießen*

⁶*The Graduate University for Advanced Studies, Hayama*

⁷*Hanyang University, Seoul*

⁸*University of Hawaii, Honolulu, Hawaii 96822*

⁹*High Energy Accelerator Research Organization (KEK), Tsukuba*

¹⁰*Institute of High Energy Physics, Chinese Academy of Sciences, Beijing*

¹¹*Institute of High Energy Physics, Vienna*

¹²*Institute of High Energy Physics, Protvino*

¹³*Institute for Theoretical and Experimental Physics, Moscow*

¹⁴*J. Stefan Institute, Ljubljana*

¹⁵*Kanagawa University, Yokohama*

¹⁶*Korea University, Seoul*

¹⁷*Kyungpook National University, Taegu*

¹⁸*École Polytechnique Fédérale de Lausanne (EPFL), Lausanne*

¹⁹*Faculty of Mathematics and Physics, University of Ljubljana, Ljubljana*

²⁰*University of Maribor, Maribor*

²¹*University of Melbourne, School of Physics, Victoria 3010*

²²*Nagoya University, Nagoya*

²³*Nara Women's University, Nara*

²⁴*National Central University, Chung-li*

²⁵*National United University, Miao Li*

²⁶*Department of Physics, National Taiwan University, Taipei*

²⁷*H. Niewodniczanski Institute of Nuclear Physics, Krakow*

²⁸*Nippon Dental University, Niigata*

²⁹*Niigata University, Niigata*

³⁰*University of Nova Gorica, Nova Gorica*

³¹*Osaka City University, Osaka*

³²*Osaka University, Osaka*

³³*Panjab University, Chandigarh*

³⁴*Saga University, Saga*

³⁵*University of Science and Technology of China, Hefei*

³⁶*Seoul National University, Seoul*

³⁷*Sungkyunkwan University, Suwon*

³⁸*University of Sydney, Sydney, New South Wales*

³⁹*Tata Institute of Fundamental Research, Mumbai*

⁴⁰*Toho University, Funabashi*

⁴¹*Tohoku Gakuin University, Tagajo*

⁴²*Department of Physics, University of Tokyo, Tokyo*

⁴³*Tokyo Institute of Technology, Tokyo*

⁴⁴*Tokyo Metropolitan University, Tokyo*

⁴⁵*Tokyo University of Agriculture and Technology, Tokyo*

⁴⁶*Virginia Polytechnic Institute and State University, Blacksburg, Virginia 24061*

⁴⁷*Yonsei University, Seoul*

We have studied $B_s^0 \rightarrow D_s^- \pi^+$ and $B_s^0 \rightarrow D_s^\mp K^\pm$ decays using 23.6 fb^{-1} of data collected at the $\Upsilon(5S)$ resonance with the Belle detector at the KEKB e^+e^- collider. This highly pure $B_s^0 \rightarrow D_s^- \pi^+$ sample is used to measure the branching fraction, $\mathcal{B}(B_s^0 \rightarrow D_s^- \pi^+) = [3.67_{-0.33}^{+0.35}(\text{stat.})_{-0.42}^{+0.43}(\text{syst.}) \pm 0.49(f_s)] \times 10^{-3}$ ($f_s = N_{B_s^{(*)}\bar{B}_s^{(*)}}/N_{b\bar{b}}$) and the fractions of B_s^0 event types at the $\Upsilon(5S)$ energy, in particular $N_{B_s^* \bar{B}_s^*}/N_{B_s^{(*)} \bar{B}_s^{(*)}} = (90.1_{-4.0}^{+3.8} \pm 0.2)\%$. We also determine the masses $M(B_s^0) = (5364.4 \pm 1.3 \pm 0.7) \text{ MeV}/c^2$ and $M(B_s^*) = (5416.4 \pm 0.4 \pm 0.5) \text{ MeV}/c^2$. In addition, we observe $B_s^0 \rightarrow D_s^\mp K^\pm$ decays with a significance of 3.5σ and measure $\mathcal{B}(B_s^0 \rightarrow D_s^\mp K^\pm) = [2.4_{-1.0}^{+1.2}(\text{stat.}) \pm 0.3(\text{syst.}) \pm 0.3(f_s)] \times 10^{-4}$.

PACS numbers: 13.25.Hw, 13.25.Gv, 14.40.Gx, 14.40.Nd

The decay $B_s^0 \rightarrow D_s^- \pi^+$ [1] has a relatively large branching fraction and is a primary normalization mode at hadron colliders, where the absolute production rate of B_s^0 mesons is difficult to measure directly. It proceeds dominantly via a Cabibbo-favoured tree process. The decay $B^0 \rightarrow D^- \pi^+$ proceeds through the same tree process but may also have additional contributions from W -exchange, so a comparison of the partial widths of the two decays can give insight into the poorly known W -exchange process. The Cabibbo-suppressed mode $B_s^0 \rightarrow D_s^\mp K^\pm$ is mediated by $b \rightarrow c$ and $b \rightarrow u$ tree transitions of similar order ($\sim \lambda^3$, in the Wolfenstein parameterization [2]), which raises the possibility of measuring time-dependent CP -violating effects [3]. It has recently become possible to produce B_s^0 events from e^+e^- collisions at the $\Upsilon(5S)$ resonance in sufficiently large numbers to achieve interesting and competitive measurements. $\Upsilon(5S)$ events may also be used to determine precisely the masses of B_s^* and B_s^0 ; the mass difference can be compared with that of B^{*0} and B^0 to test heavy-quark symmetry [4], which predicts equality between them. Properties of the $\Upsilon(5S)$ such as the fraction of events containing a B_s^0 and the relative proportions of $B_s^0 \bar{B}_s^0$, $B_s^* \bar{B}_s^0$, and $B_s^* \bar{B}_s^*$ provide additional tests of heavy quark theories [5, 6].

In this Letter, we report measurements performed with fully reconstructed $B_s^0 \rightarrow D_s^- \pi^+$ and $B_s^0 \rightarrow D_s^\mp K^\pm$ decays in $L_{\text{int}} = (23.6 \pm 0.3) \text{ fb}^{-1}$ of data collected with the Belle detector at the KEKB asymmetric-energy (3.6 GeV on 8.2 GeV) e^+e^- collider [7] operated at the $\Upsilon(5S)$ resonance. The beam energy in the center-of-mass (CM) frame is measured to be $E_b^* = \sqrt{s}/2 = 5433.5 \pm 0.5 \text{ MeV}$ with $\Upsilon(5S) \rightarrow \Upsilon(1S) \pi^+ \pi^-$, $\Upsilon(1S) \rightarrow \mu^+ \mu^-$ decays [8]. The total $b\bar{b}$ cross sec-

tion at the $\Upsilon(5S)$ energy has been measured to be $\sigma_{b\bar{b}}^{\Upsilon(5S)} = (0.302 \pm 0.014) \text{ nb}$ [9], which includes B^0 , B^+ and B_s^0 events. Three B_s^0 production modes are kinematically allowed: $B_s^0 \bar{B}_s^0$, $B_s^* \bar{B}_s^0$, and $B_s^* \bar{B}_s^*$. The B_s^* decays electromagnetically to B_s^0 , emitting a photon with energy $E_\gamma \sim 53 \text{ MeV}$. The fraction of $b\bar{b}$ events containing a $B_s^{(*)} \bar{B}_s^{(*)}$ pair has been measured to be $f_s = N_{B_s^{(*)} \bar{B}_s^{(*)}}/N_{b\bar{b}} = (19.5_{-2.3}^{+3.0})\%$ [9]. The number of B_s^0 mesons in the sample is thus $N_{B_s^0} = 2 \times L_{\text{int}} \times \sigma_{b\bar{b}}^{\Upsilon(5S)} \times f_s = (2.78_{-0.36}^{+0.45}) \times 10^6$. The B_s^0 production mode ratios are defined as $f_{B_s^* \bar{B}_s^*} = N_{B_s^* \bar{B}_s^*}/N_{B_s^{(*)} \bar{B}_s^{(*)}}$, $f_{B_s^* \bar{B}_s^0} = N_{B_s^* \bar{B}_s^0}/N_{B_s^{(*)} \bar{B}_s^{(*)}}$ and $f_{B_s^0 \bar{B}_s^0} = N_{B_s^0 \bar{B}_s^0}/N_{B_s^{(*)} \bar{B}_s^{(*)}}$. Belle previously measured $f_{B_s^* \bar{B}_s^*} = (93_{-9}^{+7})\%$ [10].

The Belle detector is a large-solid-angle magnetic spectrometer that consists of a silicon vertex detector, a central drift chamber (CDC), an array of aerogel threshold Cherenkov counters (ACC), a barrel-like arrangement of time-of-flight scintillation counters (TOF), and an electromagnetic calorimeter comprised of CsI(Tl) crystals located inside a superconducting solenoid coil that provides a 1.5 T magnetic field. An iron flux-return located outside of the coil is instrumented to detect K_L^0 and to identify muons. The detector is described in detail elsewhere [11].

Reconstructed charged tracks are required to have a maximum impact parameter with respect to the nominal interaction point of 0.5 cm in the radial direction and 3 cm in the beam-axis direction. A likelihood ratio $\mathcal{R}_{K/\pi} = \mathcal{L}_K/(\mathcal{L}_\pi + \mathcal{L}_K)$ is built using ACC, TOF and CDC (dE/dx) measurements. A track is identified as a pion if $\mathcal{R}_{K/\pi} < 0.6$ or as a kaon otherwise. With this selection, the identification efficiency for pions (kaons) is about 91% (85%), while the fake rate is about 9% (14%).

Neutral kaons are reconstructed via the decay $K_S^0 \rightarrow \pi^+\pi^-$ with no identification requirements for the two charged pions. The K_S^0 candidates are required to have an invariant mass within $\pm 7.5 \text{ MeV}/c^2$ ($\pm 4\sigma$) of the nominal K_S^0 mass (all nominal mass values are taken from Ref. [12]). Requirements on the K_S^0 vertex displacement from the interaction point and on the difference between vertex and K_S^0 flight directions are applied. The criteria are described in detail elsewhere [13]. The K^{*0} (ϕ) candidates are reconstructed via the decay $K^{*0} \rightarrow K^+\pi^-$ ($\phi \rightarrow K^+K^-$) with an invariant mass within $\pm 50 \text{ MeV}/c^2$ ($\pm 12 \text{ MeV}/c^2$) of the nominal mass.

Candidates for D_s^- are reconstructed in the three modes $D_s^- \rightarrow \phi\pi^-$, $D_s^- \rightarrow K^{*0}K^-$, and $D_s^- \rightarrow K_S^0K^-$ and required to have mass within $\pm 15 \text{ MeV}/c^2$ ($\pm 3\sigma$) of the nominal D_s^- mass for $B_s^0 \rightarrow D_s^- \pi^+$ and within $\pm 8 \text{ MeV}/c^2$ for $B_s^0 \rightarrow D_s^\mp K^\pm$. Following Ref. [10], the signals for $B_s^0 \rightarrow D_s^- \pi^+$ and $B_s^0 \rightarrow D_s^\mp K^\pm$ are observed using two variables: the beam-constrained mass of the B_s^0 candidate $M_{bc} = \sqrt{E_b^{*2} - \vec{p}_{B_s^0}^{*2}}$ and the energy difference $\Delta E = E_{B_s^0}^* - E_b^*$, where $(E_{B_s^0}^*, \vec{p}_{B_s^0}^*)$ is the four-momentum of the B_s^0 candidate expressed in the CM frame. We select candidates with $M_{bc} > 5.3 \text{ GeV}/c^2$ and $-0.3 \text{ GeV} < \Delta E < 0.4 \text{ GeV}$. In each event the B_s^0 candidate with the D_s^- mass closest to its nominal value is selected for further analysis; only $\approx 1\%$ of events have more than one candidate.

Further selection criteria are developed using Monte Carlo (MC) samples based on EvtGen [14] and GEANT [15] detector simulation. The most significant source of background is continuum events, $e^+e^- \rightarrow u\bar{u}, d\bar{d}, s\bar{s}, c\bar{c}$. In addition, for the $B_s^0 \rightarrow D_s^\mp K^\pm$ mode there is also a large background from $B_s^0 \rightarrow D_s^- \pi^+$, where the π^+ is misidentified as a K^+ . The expected continuum background, N_{bkg} , is estimated using MC-generated continuum events representing three times the data. The expected signal, N_{sig} , is obtained assuming $\mathcal{B}(B_s^0 \rightarrow D_s^- \pi^+) = 3.0 \times 10^{-3}$ and $f_{B_s^* \bar{B}_s^*} = 93\%$ for the $B_s^0 \rightarrow D_s^- \pi^+$ analysis and $\mathcal{B}(B_s^0 \rightarrow D_s^\mp K^\pm) = 3.7 \times 10^{-4}$ for the $B_s^0 \rightarrow D_s^\mp K^\pm$ analysis. For $B_s^0 \rightarrow D_s^\mp K^\pm$, we assume the values of $\mathcal{B}(B_s^0 \rightarrow D_s^- \pi^+)$ and $f_{B_s^* \bar{B}_s^*}$ obtained in the $B_s^0 \rightarrow D_s^- \pi^+$ analysis.

To improve signal relative to background, criteria are chosen to maximize $N_{\text{sig}}/\sqrt{N_{\text{sig}} + N_{\text{bkg}}}$, evaluated in the $B_s^* \bar{B}_s^*$ signal region (Fig. 1). Two topological variables are used. First, we use the ratio of the second and zeroth Fox-Wolfram moments [16], R_2 , which has a broad distribution between zero and one for jet-like continuum events and is concentrated in the range below 0.5 for the more spherical signal events. Candidates for $B_s^0 \rightarrow D_s^- \pi^+$ ($B_s^0 \rightarrow D_s^\mp K^\pm$) are required to have $R_2 < 0.5$ (< 0.4). We then use the helicity angle θ_{hel} of the $D_s^- \rightarrow \phi\pi^-$ ($D_s^- \rightarrow K^{*0}K^-$) decays, defined as the angle between the momentum of the positive daughter of the ϕ (K^{*0}) and the momentum of the D_s^- in the ϕ

(K^{*0}) rest frame; for signal decays consisting in a spin-0 particle decaying into a spin-1 particle and a spin-0 particle, the distribution is $\propto \cos^2 \theta_{\text{hel}}$, while for combinatorial background under D_s^- signal it is flat. Candidates for $D_s^- \rightarrow \phi\pi^-$ and $D_s^- \rightarrow K^{*0}K^-$ are required to satisfy $|\cos \theta_{\text{hel}}| > 0.2$ (> 0.35) for the $B_s^0 \rightarrow D_s^- \pi^+$ ($B_s^0 \rightarrow D_s^\mp K^\pm$) mode. These two selections reject 43% (73%) of the continuum while retaining 95% (85%) of the $B_s^0 \rightarrow D_s^- \pi^+$ ($B_s^0 \rightarrow D_s^\mp K^\pm$) signal. MC studies show that background from B^+ and B^0 decays is small and flat enough to be described together with the continuum events for the $B_s^0 \rightarrow D_s^- \pi^+$ mode and is negligible for the $B_s^0 \rightarrow D_s^\mp K^\pm$ mode. The most relevant background from B_s^0 decays is $B_s^0 \rightarrow D_s^{*-} \pi^+$.

For each mode, a two-dimensional unbinned extended maximum likelihood fit [17] in M_{bc} and ΔE is performed on the selected candidates, which are shown in Fig. 1. Each signal probability density function (PDF) is described by a sum of two Gaussians. For the $B_s^0 \rightarrow D_s^- \pi^+$ analysis, all three B_s^0 production modes ($B_s^* \bar{B}_s^*$, $B_s^* \bar{B}_s^0$ and $B_s^0 \bar{B}_s^0$) are fitted simultaneously. For the $B_s^0 \rightarrow D_s^\mp K^\pm$ mode, only the $B_s^* \bar{B}_s^*$ component is taken into account. The resolutions for M_{bc} and ΔE are estimated from the MC and scaled by a common factor (one for each variable) left free in the $B_s^0 \rightarrow D_s^- \pi^+$ fit. Approximating $p_{B_s^*}^*$ with $p_{B_s^0}^*$ in the $B_s^* \rightarrow B_s^0 \gamma$ decay, the mean values are parameterized, as shown in Table I, as functions of the B_s^0 and B_s^* masses, which are also left free in the $B_s^0 \rightarrow D_s^- \pi^+$ fit. The continuum (together with possible B^+ and B^0 background) is modeled with an ARGUS function [18] for M_{bc} and a linear function for ΔE . A non-parametric two-dimensional PDF, obtained from MC with the KEYS method [19], is used to describe the shape of the $B_s^0 \rightarrow D_s^{*-} \pi^+$ background.

TABLE I: Parameterization of M_{bc} and ΔE mean values.

Signal	Mean of ($M_{bc}, \Delta E$)
$B_s^* \bar{B}_s^*$	$\left(m_{B_s^*}, \sqrt{E_b^{*2} - (m_{B_s^*}^2 - m_{B_s^0}^2)} - E_b^* \right)$
$B_s^* \bar{B}_s^0$	$\left(\sqrt{\frac{m_{B_s^*}^2 + m_{B_s^0}^2}{2} - \left(\frac{m_{B_s^*}^2 - m_{B_s^0}^2}{4E_b^*} \right)^2}, -\frac{m_{B_s^*}^2 - m_{B_s^0}^2}{4E_b^*} \right)$
$B_s^0 \bar{B}_s^0$	$\left(m_{B_s^0}, 0 \right)$

For the $B_s^0 \rightarrow D_s^- \pi^+$ mode, the three signal yields are expressed as a function of three free parameters, $\mathcal{B}(B_s^0 \rightarrow D_s^- \pi^+)$, $f_{B_s^* \bar{B}_s^*}$, and $f_{B_s^* \bar{B}_s^0}$, with the relations $N_M = N_{B_s^0} \mathcal{B}(B_s^0 \rightarrow D_s^- \pi^+) f_M \sum_k \epsilon_k^M \mathcal{B}_k$ where M is one of the three $B_s^*(*) \bar{B}_s^*(*)$ -pair production modes and k runs over the D_s^- modes; the third fraction is defined as $f_{B_s^0 \bar{B}_s^0} = 1 - f_{B_s^* \bar{B}_s^*} - f_{B_s^* \bar{B}_s^0}$. The values of $\sum_k \epsilon_k^M \mathcal{B}_k$, which are the total D_s^- branching fractions [12] weighted

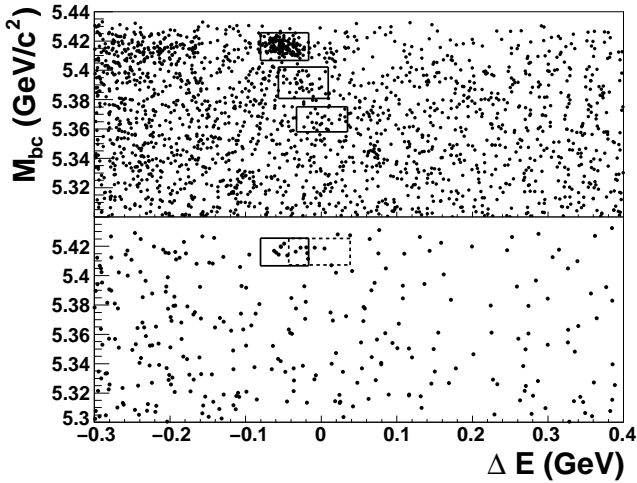


FIG. 1: $(M_{bc}, \Delta E)$ scatter plots for $B_s^0 \rightarrow D_s^- \pi^+$ (top) and $B_s^0 \rightarrow D_s^+ K^\pm$ (bottom) candidates. The three boxes in the top plot are the $\pm 2.5\sigma$ signal regions ($B_s^* \bar{B}_s^*$, $B_s^* \bar{B}_s^0$ and $B_s^0 \bar{B}_s^0$, from top to bottom) while those in the bottom plot are the $\pm 2.5\sigma$ $B_s^* \bar{B}_s^*$ regions for signal (solid) and for $B_s^0 \rightarrow D_s^- \pi^+$ background (dashed).

TABLE II: Signal efficiencies, yields (N) and significances (S).

$\Upsilon(5S)$ mode	$\sum_k \varepsilon_k \mathcal{B}_k$	N	S
$B_s^0 \rightarrow D_s^- \pi^+$ mode		161 ± 15	
$B_s^* \bar{B}_s^*$	1.58%	145_{-13}^{+14}	21.0σ
$B_s^* \bar{B}_s^0$	1.58%	$11.8_{-5.0}^{+5.8}$	2.7σ
$B_s^0 \bar{B}_s^0$	1.56%	$4.0_{-3.7}^{+4.6}$	1.1σ
$B_s^0 \rightarrow D_s^+ K^\pm$ mode			
$B_s^* \bar{B}_s^*$	1.12%	$6.7_{-2.7}^{+3.4}$	3.5σ

by the reconstruction efficiencies, are listed in Table II.

Figure 2 shows the M_{bc} and ΔE projections in the $B_s^* \bar{B}_s^*$ and in the $B_s^* \bar{B}_s^0$ regions of the data, together with the fitted function. In the M_{bc} distribution, the three signal components are present due to overlap of the signal boxes; the peak on the right (middle, left) is due to $B_s^* \bar{B}_s^*$ ($B_s^* \bar{B}_s^0$, $B_s^0 \bar{B}_s^0$) production. Table II presents the fitted signal yields as well as the significance defined by $S = \sqrt{2 \ln(\mathcal{L}_{\max}/\mathcal{L}_0)}$ where \mathcal{L}_{\max} (\mathcal{L}_0) is the value at the maximum (with the corresponding yield set to zero) of the likelihood function convolved with a Gaussian distribution that represents the systematic errors.

Systematic uncertainties on the branching fractions are shown in Table III. Those on $f_{B_s^* \bar{B}_s^*}$ and $f_{B_s^* \bar{B}_s^0}$ are mainly due to PDF uncertainties. Those due to the beam energy, the momentum calibration and the $p_{B_s^*}^* \approx p_{B_s^0}^*$ approximation are propagated as systematics on the B_s^* mass and B_s^0 mass. The momentum normalization uncertainties are much more important in the latter case because the measured energy of the B_s^0 candidate is used instead of the beam energy.

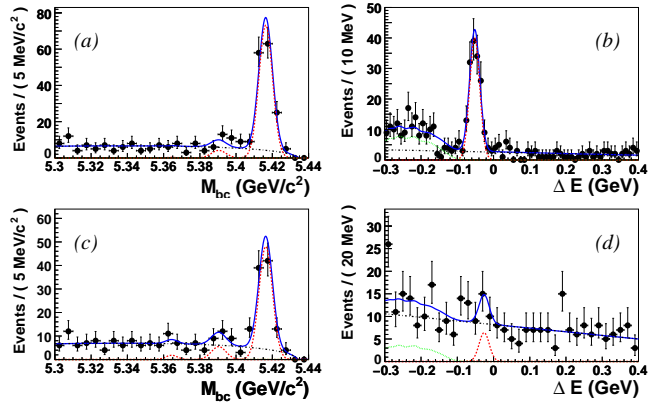


FIG. 2: (a) M_{bc} distribution of the $B_s^0 \rightarrow D_s^- \pi^+$ candidates with ΔE in the $B_s^* \bar{B}_s^*$ signal region $[-80, -17]$ MeV. (b) ΔE distribution of the $B_s^0 \rightarrow D_s^- \pi^+$ candidates with M_{bc} in the $B_s^* \bar{B}_s^*$ signal region $[5.41, 5.43]$ GeV/c^2 . The different fitted components are shown with dashed curves for the signal, dotted curves for the $B_s^0 \rightarrow D_s^- \pi^+$ background, and dash-dotted curves for the continuum. (c) and (d) shows the same distributions but using the $B_s^* \bar{B}_s^0$ signal region ($\Delta E \in [-57, 9]$ MeV and $M_{bc} \in [5.38, 5.40]$ GeV/c^2).

TABLE III: Relative systematic uncertainties (in %) for $\mathcal{B}(B_s^0 \rightarrow D_s^- \pi^+)$ and $\mathcal{B}(B_s^0 \rightarrow D_s^+ K^\pm)$.

Source	$B_s^0 \rightarrow D_s^- \pi^+$		$B_s^0 \rightarrow D_s^+ K^\pm$	
Integrated luminosity	+1.3	-1.3	+1.4	-1.2
$\sigma_{bb}^{\Upsilon(5S)}$	+4.8	-4.4	+5.0	-4.4
f_s	+13.3	-13.3	+13.6	-13.4
$f_{B_s^* \bar{B}_s^*}$	—	—	+4.8	-4.1
D_s^- branching fractions	+6.6	-6.1	+6.8	-5.9
Efficiencies (MC stat.)	+1.2	-1.2	+1.5	-1.3
Efficiencies ($R_2, \cos \theta_{\text{hel}}$)	+4.8	-4.8	+4.8	-4.8
π^\pm, K^\pm identification	+5.4	-5.4	+5.2	-5.2
Track reconstruction	+4.0	-4.0	+4.0	-4.0
PDF shapes	+1.0	-1.0	+3.3	-2.7
Total	+17.8	-17.5	+19.0	-18.1

We measure the branching fraction $\mathcal{B}(B_s^0 \rightarrow D_s^- \pi^+) = [3.67_{-0.33}^{+0.35}(\text{stat.})_{-0.42}^{+0.43}(\text{syst.}) + 0.49(f_s)] \times 10^{-3}$ where the largest systematic uncertainty, due to f_s , is quoted separately, the fraction $f_{B_s^* \bar{B}_s^*} = (90.1_{-4.0}^{+3.8} \pm 0.2)\%$ and the two fitted masses $m_{B_s^0} = (5364.4 \pm 1.3 \pm 0.7)$ MeV/c^2 and $m_{B_s^*} = (5416.4 \pm 0.4 \pm 0.5)$ MeV/c^2 . These four measurements supersede the previous Belle values [10]. We obtain for the first time values for the two fractions $f_{B_s^* \bar{B}_s^0} = (7.3_{-3.0}^{+3.3} \pm 0.1)\%$ and $f_{B_s^0 \bar{B}_s^0} = (2.6_{-2.5}^{+2.6})\%$, using the correlation (-0.77) between $f_{B_s^* \bar{B}_s^*}$ and $f_{B_s^* \bar{B}_s^0}$.

Our branching fraction is compatible with the CDF result [12, 20], and is slightly higher (1.3σ) than $\mathcal{B}(B^0 \rightarrow D^- \pi^+)$ [12]. The value of $f_{B_s^* \bar{B}_s^*}$ is significantly larger than the theoretical expectation of $\approx 70\%$ [5, 6]. The

B_s^0 mass is compatible with the world average value [12] while our value for the B_s^* mass is 2.6σ larger than the result from CLEO [21]. The mass difference obtained, $m_{B_s^*} - m_{B_s^0} = 52.0 \pm 1.5 \text{ MeV}/c^2$, is 4.0σ larger than the world average of $m_{B^{*0}} - m_{B^0}$ [12], while heavy-quark symmetry predicts equal values [4].

The distribution of the angle between the B_s^0 momentum and the beam axis in the CM frame is of theoretical interest [5] and is presented in Fig. 3 for the signal events in the $B_s^* \bar{B}_s^*$ region, using the *sPlot* method [22]. A fit to a $1 + a \cos^2 \theta_{B_s^*}^*$ distribution returns $\chi^2/\text{n.d.f.} = 8.74/8$ and $a = -0.59_{-0.16}^{+0.18}$. It has been checked that the signal efficiency does not depend on this angle. We naively expect $a = -0.27$ by summing over all the possible polarization states.

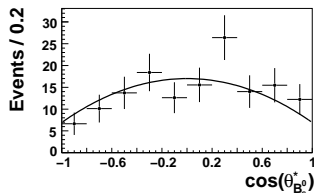


FIG. 3: Fitted distribution of the cosine of the angle between the B_s^0 momentum and the beam axis in the CM frame for the $\Upsilon(5S) \rightarrow B_s^* \bar{B}_s^*$ signal.

For the $B_s^0 \rightarrow D_s^\mp K^\pm$ mode, mean values and resolutions for $B_s^0 \rightarrow D_s^\mp K^\pm$ and $B_s^0 \rightarrow D_s^- \pi^+$ components are calibrated using the results of the $B_s^0 \rightarrow D_s^- \pi^+$ fit. The four yields (signal, continuum, $B_s^0 \rightarrow D_s^- \pi^+$ and $B_s^0 \rightarrow D_s^* \pi^+$) are allowed to float, but, due to the very small contribution of $B_s^0 \rightarrow D_s^* \pi^+$, the ratio between the yields of $B_s^0 \rightarrow D_s^* \pi^+$ and $B_s^0 \rightarrow D_s^- \pi^+$ is fixed from a fit to data without kaon identification.

The fit results are shown in Fig. 4 and Table II. Systematic errors are presented in Table III. We find $6.7_{-2.7}^{+3.4}$ signal events (3.5σ), corresponding to $\mathcal{B}(B_s^0 \rightarrow D_s^\mp K^\pm) = [2.4_{-1.0}^{+1.2}(\text{stat.}) \pm 0.3(\text{syst.}) \pm 0.3(f_s)] \times 10^{-4}$, using the previously fitted value of $f_{B_s^* \bar{B}_s^*}$. In the ratio $\mathcal{B}(B_s^0 \rightarrow D_s^\mp K^\pm) / \mathcal{B}(B_s^0 \rightarrow D_s^- \pi^+) = (6.5_{-2.9}^{+3.5})\%$, the errors are dominated by the low $B_s^0 \rightarrow D_s^\mp K^\pm$ statistics.

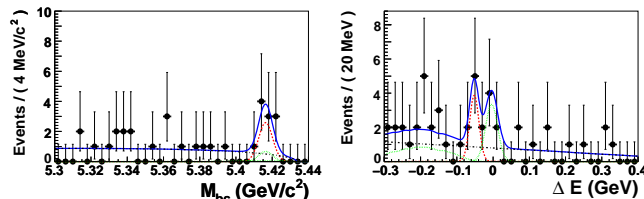


FIG. 4: Left: M_{bc} distribution of $B_s^0 \rightarrow D_s^\mp K^\pm$ candidates with ΔE in the $B_s^* \bar{B}_s^*$ signal region. Right: ΔE distribution of the $B_s^0 \rightarrow D_s^\mp K^\pm$ candidates with M_{bc} in the $B_s^* \bar{B}_s^*$ signal region; the left (right) peak is the $B_s^0 \rightarrow D_s^\mp K^\pm$ ($B_s^0 \rightarrow D_s^- \pi^+$) component. The dashed, dotted and dash-dotted curves represent the signal, $B_s^0 \rightarrow D_s^{(*)-} \pi^+$ backgrounds, and continuum, respectively.

In summary, a large $B_s^0 \rightarrow D_s^- \pi^+$ signal is observed and six physics parameters are measured: the branching fraction $\mathcal{B}(B_s^0 \rightarrow D_s^- \pi^+) = [3.67_{-0.33}^{+0.35}(\text{stat.})_{-0.42}^{+0.43}(\text{syst.}) \pm 0.49(f_s)] \times 10^{-3}$, the fractions of the B_s^0 pair production modes at the $\Upsilon(5S)$ energy, $f_{B_s^* \bar{B}_s^*} = (90.1_{-4.0}^{+3.8} \pm 0.2)\%$, $f_{B_s^* \bar{B}_s^0} = (7.3_{-3.0}^{+3.3} \pm 0.1)\%$, $f_{B_s^0 \bar{B}_s^0} = (2.6_{-2.5}^{+2.6})\%$, and the masses $m_{B_s^*} = (5416.4 \pm 0.4 \pm 0.5) \text{ MeV}/c^2$, $m_{B_s^0} = (5364.4 \pm 1.3 \pm 0.7) \text{ MeV}/c^2$. In addition, evidence (3.5σ) for the $B_s^0 \rightarrow D_s^\mp K^\pm$ decay is obtained, leading to a measurement $\mathcal{B}(B_s^0 \rightarrow D_s^\mp K^\pm) = [2.4_{-1.0}^{+1.2}(\text{stat.}) \pm 0.3(\text{syst.}) \pm 0.3(f_s)] \times 10^{-4}$.

We thank the KEKB group for excellent operation of the accelerator, the KEK cryogenics group for efficient solenoid operations, and the KEK computer group and the NII for valuable computing and SINET3 network support. We acknowledge support from MEXT and JSPS (Japan); ARC and DEST (Australia); NSFC (China); DST (India); MOEHRD, KOSEF and KRF (Korea); KBN (Poland); MES and RFAAE (Russia); ARRS (Slovenia); SNSF (Switzerland); NSC and MOE (Taiwan); and DOE (USA).

* now at Okayama University, Okayama

- [1] Unless specified otherwise, charge-conjugated modes are implied throughout the Letter.
- [2] L. Wolfenstein, Phys. Rev. Lett. **51**, 1945 (1983).
- [3] R. Aleksan, I. Dunietz and B. Kayser, Z. Phys. C**54**, 653 (1992). See also R. Fleicher, Nucl. Phys. B **671**, 459 (2003) and S. Nandi and U. Nierste, Phys. Rev. D **77**, 054010 (2008).
- [4] W.A. Bardeen, E.J. Eichten and C.T. Hill, Phys. Rev. D **68**, 054024 (2003).
- [5] A.G. Grozin and M. Neubert, Phys. Rev. D **55**, 272 (1997).
- [6] N.A. Törnqvist, Phys. Rev. Lett. **53**, 878 (1984).
- [7] S. Kurokawa and E. Kikutani, Nucl. Instrum. Methods A **499**, 1 (2003).
- [8] K.-F. Chen *et al.* (Belle Collaboration), Phys. Rev. Lett. **100**, 112001 (2008). We obtain $\sqrt{s} = m_{\Upsilon(1S)} + \Delta M$ where $m_{\Upsilon(1S)}$ is the nominal $\Upsilon(1S)$ mass [12] and ΔM is the measured $M_{\mu^+ \mu^- \pi^+ \pi^-} - M_{\mu^+ \mu^-}$.
- [9] A. Drutskoy *et al.* (Belle Collaboration), Phys. Rev. Lett. **98**, 052001 (2007), G. S. Huang *et al.* (CLEO Collaboration), Phys. Rev. D **75**, 012002 (2007). These two published values of $\sigma_{bb}^{\Upsilon(5S)}$ are averaged. Experimental f_s values are also given by both of them; the average is given in Ref. [12].
- [10] A. Drutskoy *et al.* (Belle Collaboration), Phys. Rev. D **76**, 012002 (2007).
- [11] A. Abashian *et al.* (Belle Collaboration), Nucl. Instrum. Methods A **479**, 117 (2002).
- [12] C. Amsler *et al.* (Particle Data Group), Phys. Lett. B **667**, 1 (2008).
- [13] F. Fang, Ph.D. thesis, University of Hawaii (2003).
- [14] D.J. Lange, Nucl. Instrum. Methods A **462**, 152 (2001).
- [15] CERN Application Software Group (1993), CERN Program Library, W5013.

- [16] G.C. Fox and S. Wolfram, Phys. Rev. Lett. **41**, 1581 (1978).
- [17] R. Barlow, Nucl. Instrum. Methods A **297**, 496 (1990).
- [18] H. Albrecht *et al.* (ARGUS Collaboration), Phys. Lett. B **185**, 218 (1987).
- [19] K. Cranmer, Comput. Phys. Commun. **136**, 198 (2001).
- [20] A. Abulencia *et al.* (CDF Collaboration), Phys. Rev. Lett. **98**, 061802 (2007).
- [21] O. Aquines *et al.* (CLEO Collaboration), Phys. Rev. Lett. **96**, 152001 (2006).
- [22] M. Pivk and F.R. Le Diberder, Nucl. Instrum. Methods A **555**, 356 (2005).